RESEARCH ARTICLE   **Open Access**

New Zealand Journal of Forestry Science

History of slope instability in the Oldina plantation, Tasmania

Adrian Slee and Peter D. McIntosh

Forest Practices Authority, 30 Patrick Street, Hobart 7000, Australia

*Corresponding author: adrian.slee@fpa.tas.gov.au

Abstract

Background: This paper describes a landslide swarm generated by exceptionally high two-day rainfall (c. 300 mm) associated with a stationary cut-off low pressure system over northern Tasmania in early June 2016 and investigates evidence for previous slope instability. The landslide swarm occurred in a recently harvested plantation in the Inglis River catchment at Oldina, south of Wynyard in north-west Tasmania. Within a relatively small area of plantation underlain by weathered Permian tillite and minor siltstones more than thirty rapid earthflows, rotational and translational landslides occurred. Many landslides also occurred in the nearby Forth and Mersey River catchments.

Methods: Field observations combined with a digital elevation model produced from high-resolution drone imagery were used to describe the morphology of the Oldina landslides, and to calculate the mass of soil, sediment, and woody debris displaced. Radiocarbon dating of charcoal exposed in landslide backwalls enabled palaeo-landslides and periglacial activity at Oldina to be dated.

Results: An estimated 48,400–72,310 t of soil, sediment and woody debris was carried downslope by the major landslides but has been retained within the plantation area. The total sediment loss from the affected upper catchments is likely to be greater than the above estimate as the contribution from small riparian landslides, sheet, gully, and rill erosion has not been accounted for, nor has streambank erosion and sediment transported off the study site been measured. Radiocarbon dating of charcoal in sediments indicated that two landslides had evidence of previous instability in the Holocene. Most ages indicated that previous instability dated to 35–15 cal ka BP, i.e., to a time when the climate was cold and dry and freeze-thaw processes in a sparsely vegetated landscape were active.

Conclusions: During planning for harvest the soils developed on Permian tillite were correctly described as having a low to moderate risk of landslide erosion. This study concludes that the landslides initiated in June 2016 resulted from exceptionally heavy rain falling on harvested steep and hilly land coupled with the decline in root strength of the harvested trees. The frequency of such a combination of circumstances may increase if high-intensity rainfall increases in Tasmania as the result of climate change. To improve the long-term stability of this terrain and the overall sustainability of plantation forestry it is recommended that landslides and riparian areas are seeded with native vegetation, and that the current assessment of landslide risk for this terrain is re-evaluated.

Keywords: Climate change; drone imagery; grèze litées, high-intensity rainfall; Holocene; landslides;
Pinus radiata plantations; radiocarbon dating

Introduction

During 5–6 June 2016 a strong slow moving depression with a north-south path similar to a cut-off East Coast Low (ECL) (Pook et al. 2010; Dowdy et al. 2011) entered Bass Strait and led to intense rainfall over northern Tasmania (Fig. 1). On 6 June 278.6 mm of rain was recorded at Fisher River at 1140 m above sea level (asl) in the Mersey River catchment, the highest 24 h rainfall total (to 9 a.m.) recorded in Tasmania during the event, and the 2-day rainfall total at this weather station was 399.2 mm (Bally 2016).

The high rainfall triggered numerous landslides (Bally 2016; Fig. 2) and accelerated karst development on agricultural and forested land (Slee et al. 2019; Burke et al. 2020) elsewhere in northern Tasmania. Severe erosion occurred in the middle Mersey and
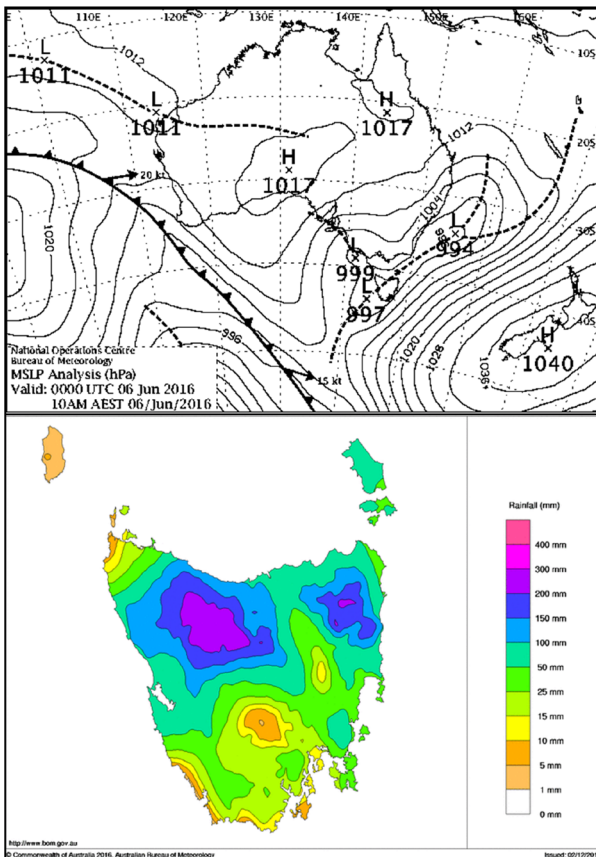
FIGURE 1: Maps of sea level atmospheric pressure and rainfall on 6 June 2016. Note the complex low-pressure systems 'trapped' between a high pressure centred on New Zealand and a high pressure centred on the Australian mainland. Maps are adapted from Bally (2016).
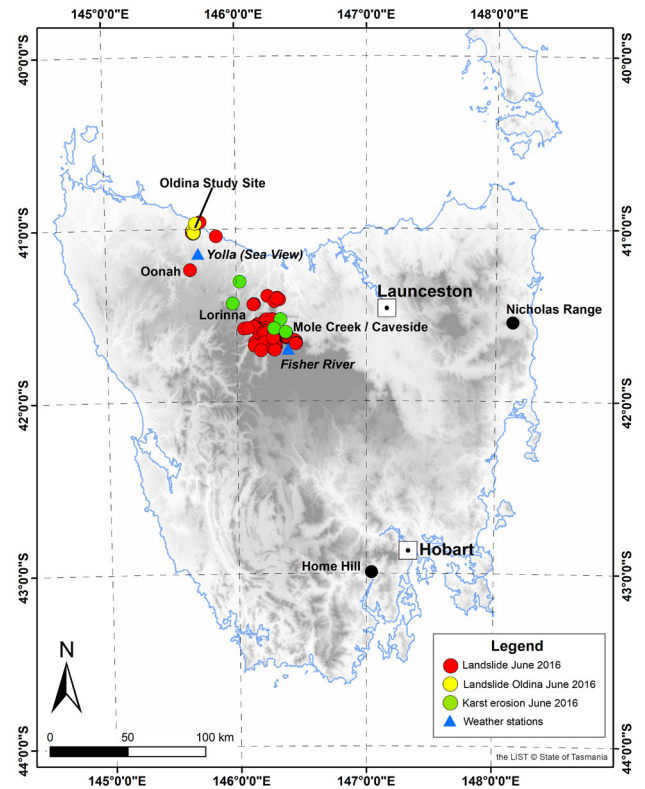

FIGURE 2: Map of Tasmania showing the distribution of the June 2016 landslides, karst erosion, other landslides, and locations mentioned in the text.

Forth catchments (Fig. 2) near Lorinna, Cethana and Caveside, where landslides damaged roads and other infrastructure (Wirsu 2017). At Caveside several landslides were mapped and described (Kaine et al. 2017, 2018), including a large earthflow originating on the upper slopes of the Great Western Tiers which deposited a 1-m thick fan on a farm paddock. At the nearby Maracoopa Cave, bouldery coarse sediment was transported by floodwaters through the cave, impacting cave landforms and damaging infrastructure (Eberhard 2016) while a landslide threatened a house near the coast on Table Cape (Bermingham 2016).

Intense rainfall extended over the northwest of the state with Yolla (Sea View) weather station 18 km south of Wynyard registering 300.2 mm of rain over 5–6 June (Bureau of Meteorology 2016). In the Oldina Plantation near Wynyard (41°01'04"S: 145°40'49"E) the exceptional rainfall triggered over 30 landslides, mostly within an 87-ha forest coupe that had been harvested in the spring and early summer of 2015/2016, but not replanted. No landslides were detected during coupe planning or early harvest. Google Earth imagery dated 10 October 2015 and earlier showed no evidence of landslides. The landslides were reported to the Forest

Practices Authority (FPA) geoscientists by a forester on 9 June 2016 following a routine inspection of the plantation and roads. Landslides also occurred in both harvested and young regrowth plantation coupes at Oonah (McIntosh 2016). Other than roadside batter failures, very few landslides were noted in the Oldina area on slopes within areas of standing native forest.

Dated slope deposits in Tasmania

Although parts of Tasmania have been recognised and mapped as being landslide prone (Mazengarb & Stevenson 2010; Stevenson 2011), there are few detailed reports or articles on landside frequency in the state, or in mainland Australia (Panek et al. 2015), notable exceptions being the work by Nott et al. (2001), Miner et al. (2011) and Tulau et al. (2019). Although landslides are common in the coastal and lower-altitude river valleys of Tasmania (Mineral Resources Tasmania 2021) and detailed hazard mapping has been undertaken in some of these areas (Mazengarb et al. 2013), a significant proportion of mountain slope deposits are associated with periglacial processes (Caine 1983; Barrows et al. 2004; McIntosh & Barrows 2011; McIntosh et al. 2012; Slee & Shulmeister 2015) and can be considered to be relict and stable in the present warm and wet climate and forested landscape. For example, on the slopes of the Mt Nicholas Range in north-eastern Tasmania, at 600–700 m asl, large landslides, extending almost 1 km from their source backwalls, form a 'ripple' landscape composed of transverse ridges, within which constituent

boulders have been dated by cosmogenic methods to have been moved to their present position in Marine Isotope Stage (MIS) 5c and 4 (McIntosh & Barrows 2011; Slee et al. 2017). These authors suggested that the landslides formed as a result of snow melt saturating the ground and inducing mass movement, but that under the current climate and forest cover the landscape is likely to remain stable. Although deposits dating to MIS 3 and 4 have been described in the backwalls of recent landslides in the Huon and Derwent catchments, the processes causing instability during cold (glacial) periods and the Holocene are different (McIntosh et al. 2009, 2012).

As most Oldina landslides occurred in a recently harvested coupe and impacted access roads and stream catchments, earth science specialists at the Forest Practices Authority (FPA) were consulted by the plantation management company to assess the damage and provide advice on measures that could be taken to stabilise eroded slopes. During field work charcoal was noted within sediments exposed in the backwalls of recently failed landslides. Radiocarbon dating of this charcoal presented an opportunity to test the hypotheses that slopes previously considered to have a low risk of mass movement under the present climate had failed previously during the Holocene, and that the soils concerned are more prone to mass movement than previously recognised in the Tasmanian Forest Practices Code (FPA 2015, 2020), which governs plantation management in Tasmania.

Aim
This paper describes the morphology of landslides triggered across a harvested coupe located within the Oldina plantation during high rainfall in 2016. We estimate the mass of displaced soil, sediment, and woody debris within the study site, describe the process of landscape evolution as revealed by stratigraphic observations and ^{14}C ages obtained from deposits exposed in the headwalls of large-scale landslides, and assess the implications of our findings for forestry as a sustainable land use in this terrain.

Methods
Study site
The study site lies in the northern part of the Oldina plantation managed by Timberlands Pacific Pty Limited (TPPL). It consists of 3577 ha of *Pinus radiata* D.Don and associated native forest reserves. The plantation was established in the 1930s and 1940s (Elliott et al. 2008; Elliott 2011) on low hills up to 210 m above sea level (asl) in the Inglis River catchment which extends south of the town of Wynyard on Tasmania's northern coastline. After harvest of these trees in the mid-1980s a second rotation was planted, and subsequently harvested in the mid-2010s. The trees at the 87 ha study site were harvested over the summer of 2015/2016 but the coupe had not been replanted when heavy rain fell in June 2016.

The plantation is mostly planted on soils developed in the sub-horizontal Wynyard Formation (Everard 2004), a mixture of marine siltstone sequences with dropstones and varved tillite that accumulated during the Permian glaciation (Henry et al. 2012). Bedding within the formation is weakly developed and the overall structure is massive. Tertiary basalt outcrops extensively south and east of the study site, and outliers occur on some of the higher ridges within the Oldina plantation (Everard 2004; Everard & Calver 2006). These outcrops are remnants of extensive flood basalts that erupted over broad areas of northern Tasmania during the Oligocene and Miocene epochs (Sutherland and Wellman 1986).

The Permian and Tertiary geological units govern topographic relief. Where the Wynyard group outcrops, topography is dominated by elongate south–north ridges rising 220 m above the coastal plain, separated by flat-floored alluvial valleys with steep sides. Local relief exceeds 140 m and interfluvial ridges are drained by numerous headwater streams defined as class 4 streams (catchments < 50 ha) in the FPA classification (Forest Practices Code 2015, 2020). Broad basalt-topped ridges separated by steep-sided gullies rise to over 350 m asl south of the plantation.

The Wynyard formation produces well-structured stony gradational soils (Grant et al. 1995, p. 76) provisionally classified as Dystric Cambisols (FAO 2014). Mottled soils (Gleyic Dystric Cambisols) occur in lower landscape positions and in depressions. Grant et al. (1995, p. 77) classified the risks of landslides and soil erosion in these soils as negligible to moderate. The basalts produce thick well-structured and well-drained brown gradational soils (Grant et al. 1995, p. 94) provisionally classified as Ferralsols (FAO 2014). Basalt colluvium may contribute to the Cambisols downslope but does not form a distinct layer.

Mean annual rainfall at Wynyard airport is 974 mm and the mean minimum and maximum June temperatures are 4.1°C and 13.5°C respectively (Bureau of Meteorology 2021a). The rainfall record at Yolla (Sea View) meteorological station (mean annual rainfall 1448 mm), 12 km south of the study site, extends almost continuously back to 1907, and reveals that the rainfall on 6 June 2016 (248 mm) was unprecedented, being the highest on record and 100 mm more than the previous daily record for the station set in 1953 (Bureau of Meteorology 2021a, b).

Landslide identification and classification
Landslides were identified from photography taken using a camera mounted on a fixed-wing 'Forest Mapper' drone operated by Australian UAV Pty Ltd, Melbourne, Victoria, producing a georeferenced image identifying ground features to c. 3–5 cm horizontal and vertical resolution (Fig 3). A digital elevation model (DEM) was developed from this imagery (Fig. 4). The length, width, and area of the landslides at the study site were interpreted from aerial imagery and summarised in excel spreadsheets. Slope changes were calculated from the drone-generated DEM using ARC-GIS. Classification of landslides followed the guidelines produced for Tasmania by Mazengarb & Stevenson (2010), based on the United States Geological Survey Landslide Fact sheet (USGS 2004). Three dominant landslide classes were
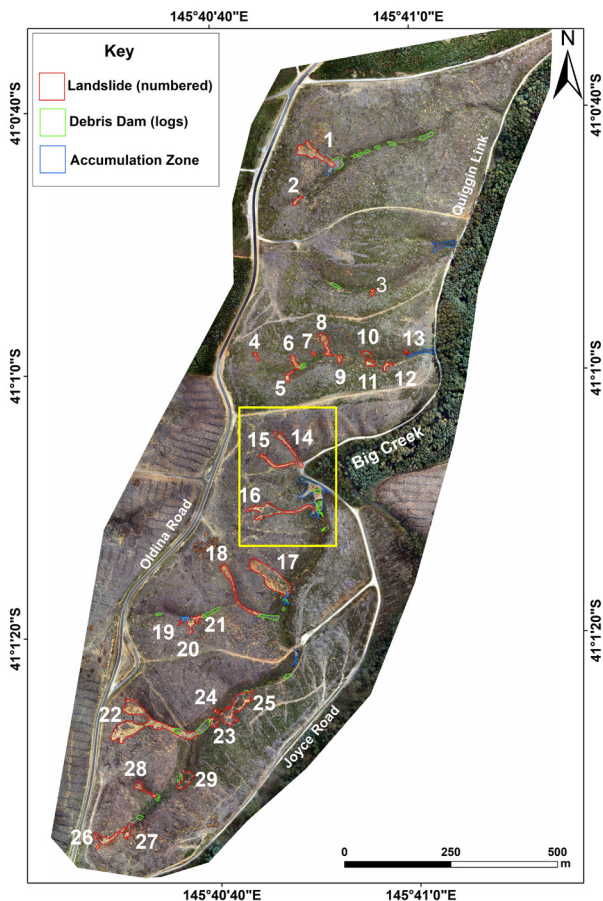
FIGURE 3: Incidence of landslides in the study site. The area shown in Figure 7 is indicated by the yellow box.

FIGURE 4: Slope map of the study site showing the relationship between the landslides and slopes >26°.

recognised: shallow earthflows, translational landslides, and rotational landslides (Fig. 5). Their length/width/area relationships are shown as a balloon diagram (Fig. 6). Large log jams formed of a mix of sediment and woody material mobilised from slopes by landslides into the trunk valleys were also mapped.

Although pre-June 2016 LiDAR imagery was available, its resolution was insufficient to allow comparison with the DEM obtained in this study.

Estimates of sediment and log jam mass

The mass of material displaced by landslides was estimated from field observations, the DEM developed from the drone imagery, and published soil bulk density measurements.

Based on observations of the height of the headwall scarps of landslides, it was estimated that the mean depth of the landslide scars in sediment source areas was approximately 2.5 m. The length of landslide debris trails/tails extending downslope of the landside scars was on average twice the length of the erosion scars themselves, and had a mean depth of about 1–1.5 m. The bulk density of tillite/siltstone soils was assumed to be 1.6 t m³, as determined for the clayey B horizon of the Roebuck soil developed in weathered Permian tillite (Hill et al. 1995, p. 279). The mass of material displaced
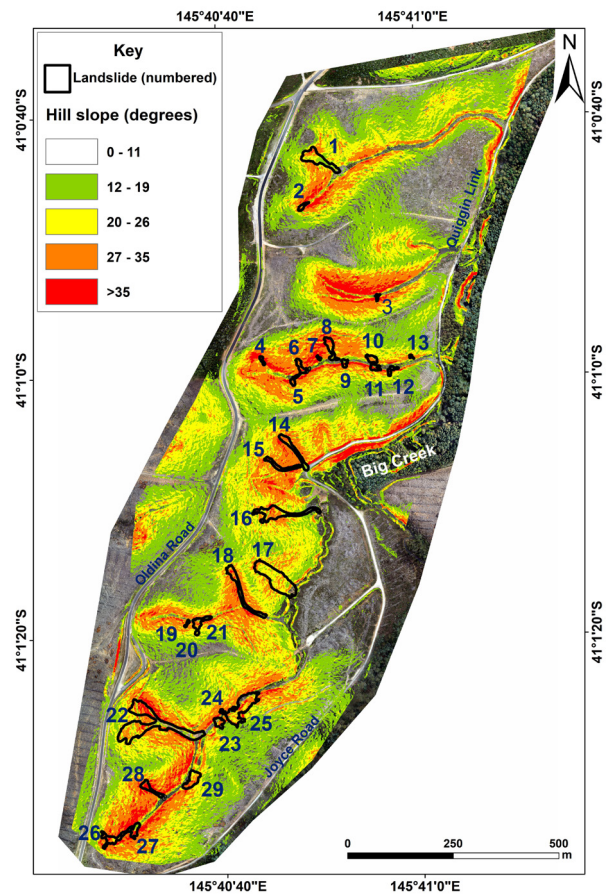
by landslides was calculated on the assumption that landslide spoil consists of clayey and stony material in the ratio 3:1 and tillite stones have a density of 2.5 t m⁻³ (Long & Menkiti 2007). The depth of material accumulated on floodplains was unknown and the mass of sediment deposited on floodplains was not calculated.

Log jams were in places more than 2 m deep but as the depth of most of the log jams could not be measured, we conservatively estimated their average depth to be 1 m. Observations indicated that between 30 and 50% of the log jam volume consisted of a silty clay matrix and the balance consisted of densely packed logs (mostly *P. radiata* debris). Calculation of the mass of material contained within log jams was based on a bulk density of 1.6 t m³ for the clayey matrix (Hill et al. 1995, p. 279) and a wood density estimate of 500 kg m⁻³ (Dale-Glass Industries 2021).

¹⁴C radiocarbon dating

The backwalls of all major landslides were inspected to assess whether they contained evidence of previous mass movement. A prominent palaeosol was evident in the backwall of landslide 22. Buried charcoal was identified in landslides 1, 6, 8, 18, 22 and 23 (Fig. 3) and submitted for standard or AMS ¹⁴C radiocarbon dating at the University of Waikato Radiocarbon Laboratory, New
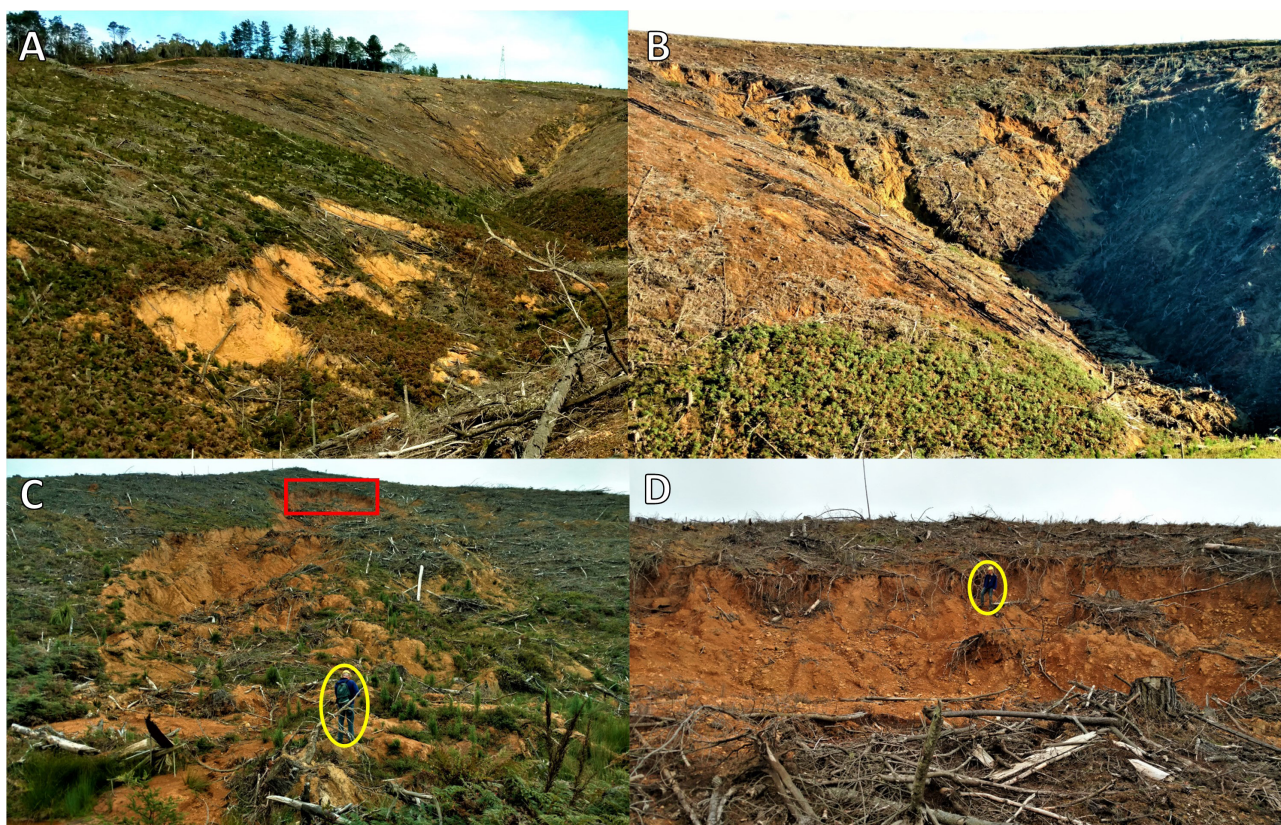
FIGURE 5: Landslide types at Oldina. A. Landslide 25, a large rotational landslide on a valley side. B. Landslide 22, a shallow elongate earthflow. C. Landslide 17, a large translational landslide with an upper rotational zone; figure for scale (circled); from the photographer to the backwall (indicated by red rectangle) is 100 m. D. The backwall of landslide 17 (a rotational landslide in this upper zone), indicated in image C by the red rectangle; figure for scale (circled).

Zealand (Table 1) after all visible contaminants such as modern roots, organic fragments and fungal hyphae had been removed during examination under a binocular microscope. Ages obtained were calibrated using OxCal version 4.4 and SHCal 20 (Bronk Ramsey 2009; Hogg et al. 2020).

Rainfall thresholds for landslide initiation
As the exact time of landslide occurrence resulting from the rain on 5–6 June 2016 is not known, and the nearest Bureau of Meteorology rain gauge is 5 km north of the study site at Wynyard airport on the coastal plain, and records here have only been collected since 1993, rainfall thresholds for landslide initiation (e.g., Peruccacci et al. 2017) have not been estimated.

Results
Landslide characteristics and dating
Mapping using aerial imagery and ground truthing identified 29 active landslides in the study site, having a combined area of 24,955 m^2 (Fig. 3). The smallest (landslide 13) was 13 m long with an area of 42 m^2 and the largest (landslide 22) was 216 m long with an area of 5657 m^2 (Fig. 6). Most of the landslides are significantly longer than they are broad – these are shallow earthflows (e.g., landslide 22; Fig. 6). Rotational

landslides are generally short where they occur next to streams (e.g., landslides 20, 21 and 25, Fig. 5A) and broader than they are long (e.g., landslide 25; Fig. 6). Landslide 17, the second most extensive on the site (3583 m^2), has a morphology of a rotational landslide in its upper part and an earthflow in its lower part (Fig. 5C and D; Fig. 6). It is nonetheless classed as a translational landslide because failure has occurred along a shallow (<2.5m deep) bedrock slip plane akin to that of the well documented translational landslide at Home Hill in southern Tasmania (Mazengarb & Stevenson 2010, figure 23; McIntosh et al. 2012; Lucieer et al. 2013; Turner et al. 2015).

With the exclusion of landslides 16 and 17, most of the mapped landslides are associated with slopes >26° classified as very steep (Fig. 4 above and also table 4 in Forest Practices Code 2020), flanking incised class 4 streams (Forest Practices Code 2015, 2020). Stream floodplains are typically flat-bottomed and infilled with sediment (Figs. 3 and 5b). It is also notable that not all steep to very steep land displayed instability following the June 2016 rain. For example, the steep areas upslope of landslide 3, east of landslide 14 and above landslide 19 (Fig. 3) all remained stable even though overall morphology of these areas suggests that the basins are a product of past mass movement.
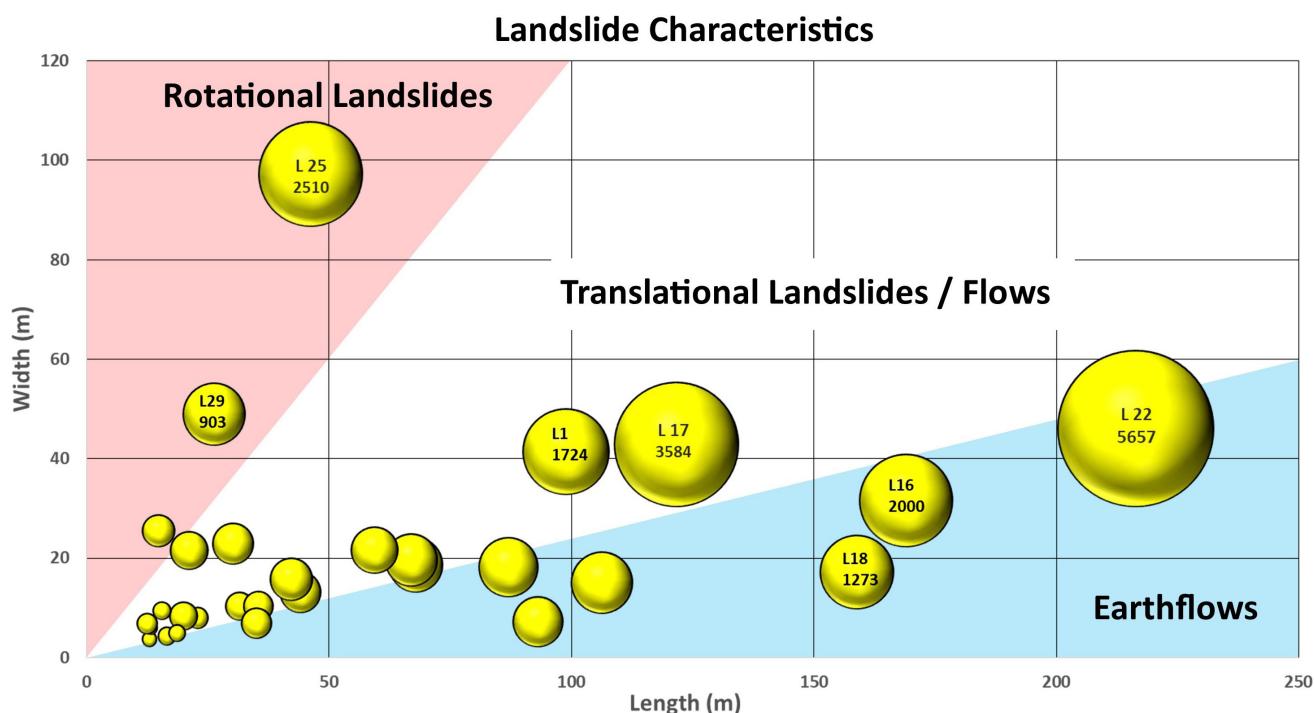
Landslide Characteristics

FIGURE 6: Length and width characteristics of the landslides within the study site with three broadly-defined zones defined by landslide-formation processes. The landslide surface areas are indicated by the size of the circles. Larger landslides are identified by number (see Figs. 4 and 5) and area.

Tracks and roads

At a limited number of sites, old farm tracks or snig tracks (timber extraction tracks) may have concentrated and redirected water into hillside depressions leading to soil saturation and the triggering of landslides such as at landslide 16 (Fig. 7). At landslide 15 (Fig. 7) drainage and landslide sediment has been diverted along an old track.

Landslide 1

Charcoal was sampled at depths of 0.7 m and 1.7 m from two layers within an exposure at the confluence of the earthflow and a class 4 stream. Both layers consist of stony silty clays with weakly developed structure. The layers were demarcated by prominent basal bands of charcoal. The deeper layer was significantly redder, stonier and more compact than the upper layer. The ^{14}C ages obtained indicate periods of slope instability during MIS 3 (34.75 cal ka BP) and during the Last Glacial Maximum (LGM) within MIS 2 (20.30 cal ka BP; Table 1) .

Landslide 6

Charcoal sampled from stony colluvium at c. 1.7 m depth (labelled B in Fig. 8) with a median ^{14}C age of 14.94 cal ka BP (Table 1) indicates previous mass movement at this site during the MIS 2 de-glacial period.

Landslide 8

Three layers were identified in the sidewall of Landslide 8 (Fig. 9). The upper 1.3 m is a stony clay containing no charcoal. The middle layer, a stony clay 1.3 m thick which displays fine bedding and imbrication of stones indicative of fluvial deposition, contains scattered

charcoal fragments with a median age of 15.58 cal ka BP (Table 1), and is considered to result from sheet erosion following a fire. The lowermost layer is a stony clay also containing scattered charcoal fragments having a median age of 27.45 cal ka BP (Table 1); stones are angular and chaotically distributed. Both ages obtained fall into MIS 2.

Landslide 18

Landslide 18 is within an eroded stream channel partly covered with stony debris from a June 2016 landslide, which has buried two layers of older debris differentiated by their colour, compactness and charcoal-rich layers in their upper parts (Fig. 10). Layer 3 was deposited at 1.05 cal ka BP and layer 2 was deposited at 0.18 cal ka BP (Table 1), i.e. both deposits formed in the late Holocene.

Landslide 22

The landslide backwall (Fig. 11) exposed a prominent charcoal-rich band dated 1.94 cal ka BP (Table 1). The charcoal-rich band is probably a former topsoil, and the associated reddened clasts are indicative of an intense bushfire that occurred before this site was buried by landslide debris about 2000 years ago. The overlying deposit (1.1 m thick) with a 30-cm-thick pale A2 horizon (McDonald et al. 1998, p.105) post-dates the landslide and is uncharacteristic of most soils in the area.

Landslide 23

Landslide 23 is a short (20 m) earthflow in the steep riparian zone of a small stream. It has a well-developed semicircular backwall formed by the collapse of about 2.5 m of stratified scree (grèze litées of García-Ruiz et al.

TABLE 1: Radiocarbon ages of charcoal in Oldina landslide backwalls and at Home Hill (McIntosh et al. 2012).

Sampled ID[1]	Landform (2021)	Inferred palaeo-process	^{14}C age[2] (^{14}C ka BP)	Method	Median Calibrated age (OxCal)[3]; range in parenthesis (cal ka BP)
Landslide 1 Lower Wk-49488	Earth flow	Uncertain; fire	30.263±0.290	AMS	34.75 (35.274–34.229)
Landslide 1 Upper Wk-49489			16.823±0.060	AMS	20.30 (20.119–20.474)
Landslide 6 WK-49490	Earth flow	Uncertain; fire	12.569±0.036	AMS	14.94 (14.794–15.094) (65%)
Landslide 8 Middle Wk-49491	Earth flow	Sheet erosion; fire	13.060±0.036	AMS	15.58 (15.401–15.764)
Landslide 8 Lower Wk-49492			23.157±120	AMS	27.45 (27.225–27.673)
Landslide 18 Layer 2 Wk-46561	Earth flow	Landslide; fire	0.201±0.027	Standard	0.18 (0.136–0.232) (56%)
Landslide 18 Layer 3 Wk-46562			1.186±0.016	AMS	1.05 (1.042–1.068) (73%)
Landslide 22 Wk-45744	Earth flow	Landslide; fire	2.027±0.025	Standard	1.94 (1.884–2.002)
Landslide 23 Wk-49493	Stratified scree	Periglacial freeze-thaw; fire	13.854±0.040	AMS	16.77 (16.584–16.973)
Home Hill Wk-22695	Stratified scree	Periglacial freeze-thaw; fire	18.060±0.109	AMS	21.94 (21.659–22.224) (87%)
Home Hill Wk-22696			20.675±0.120	AMS	24.86 (24.501–25.216)
Home Hill Wk-24895			21.596±0.114	AMS	25.86 (25.696–26.013)

[1] Wk = Waikato Radiocarbon Dating Laboratory (New Zealand).

[2] Laboratory values as reported (not rounded).

[3] Median ages rounded to the nearest 10 yr, with the 95% probability range (as reported) in parentheses, except where otherwise indicated.

(2001) and Sharples (1997, p. 48)) composed primarily of interstratified fine angular gravels formed from finely fractured Permian siltstones and mudstones ('frittered mudstones' of Lynn & Crippen (1991)). Charcoal within the gravels was dated 16.77 cal ka BP (Table 1) (Fig. 12).

Landslide mass

Using the methods and assumptions outlined in the Methods section above, it is estimated that in June 2016 45540–68310 t of sediment was carried downslope by the major landslides. More sediment is likely to have been moved as the above estimate does not take into account small riparian landsides, or sheet, gully and rill erosion, or downstream sedimentation, or sediment carried off-site in suspension.

During the field survey 24 log jams (Figs. 3 & 13) were found, mostly within valley floors close to toes of landslides. Their estimated area was 3574 m^2. The mass of wood present was estimated to be between 535 and 895 t and the mass of soil and sediment was estimated to be between 2860 and 4000 t. Adding these figures to the

estimated landslide mass produces an approximate total mass of material displaced by landslides, and remaining in the study area, of between 48400 and 72310 t.

On several of the major streams, landslide-generated sediment from higher in the catchment accumulated on floodplains behind log jams and upstream of confluences of tributary streams. The largest sediment impoundment, covering an area of 2285 m^2, was the result of a road culvert being blocked by landslide sediment, which created a sediment trap at Big Creek (blue dot in Fig. 7 and inset) which retained most landslide debris on site.

Discussion

Before the events of June 2016, soils developed in Permian tillite bedrock in Tasmania were not generally considered to be vulnerable to the initiation of landslides triggered by high rainfall. However, the landslides triggered at Oldina in June 2016 suggest that this Permian tillite terrain is indeed susceptible to landsliding albeit most likely only during or after exceptional rainfall, on slopes >26 degrees, and on clearfelled sites.
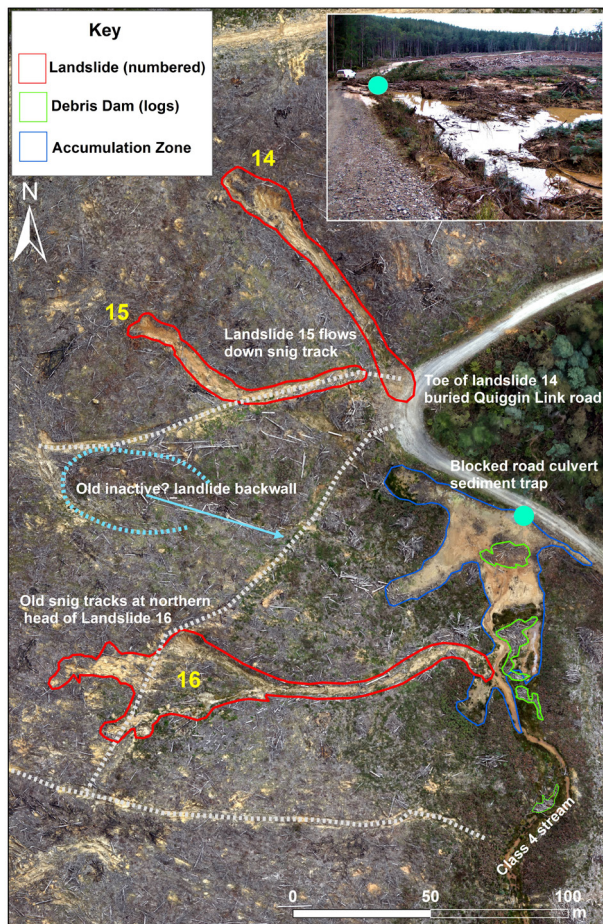
FIGURE 7: Influence of roads, snig tracks (timber extraction tracks) and blocked culverts (green dot in main image and inset image) on landslide initiation and debris accumulation.
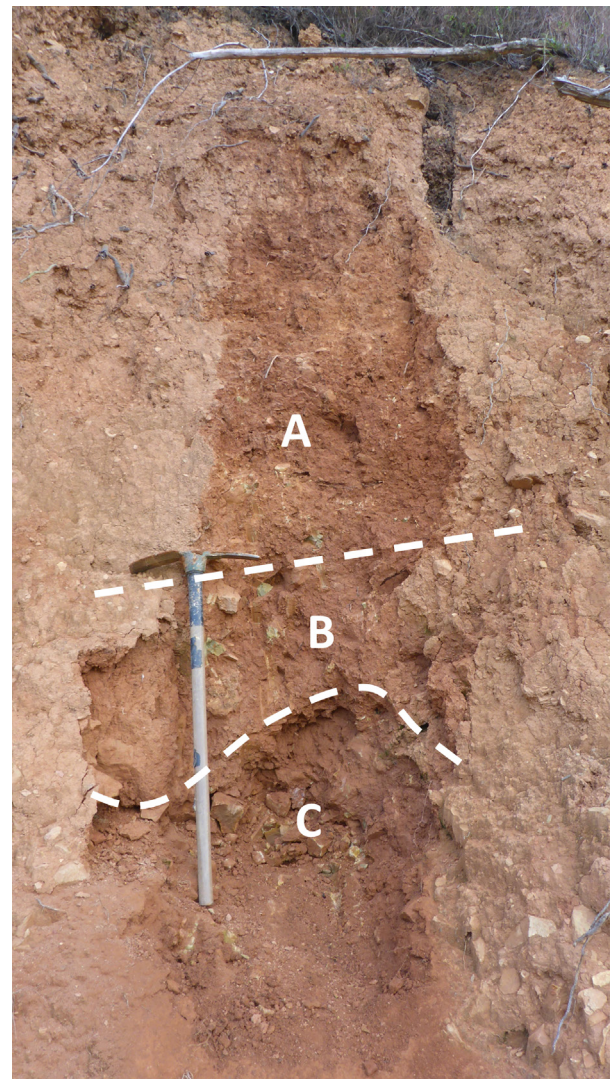

FIGURE 8: Landslide 6, backwall. Three layers are evident: a 1.3 m layer of gravelly silty clay (A), overlying a 30–50 cm deep layer of stony silty clay containing scattered charcoal fragments (B) dated 14.94 cal ka BP, overlying a very stony silty clay deposit (C).

Landslides initiated in June 2016 represent the youngest of three periods of slope instability recorded at Oldina during the Holocene epoch, at a time when the climate was warm and wet, and the landscape mostly forested, soils are likely to have been mostly stable. The evidence of dated charcoal collected from the headwalls of landslides 18 (0.18 cal ka BP and 1.05 cal ka BP) and 22 (1.94 cal ka BP), and the presence of layers of reddened soils and clasts indicative of hot fires (Ulery & Graham 1993; Hirsch et al. 2018) suggest that any slope instability during the Holocene was probably induced by natural fires and possibly the result of land clearance during early 19th century European colonisation rather than by climatic factors.

Other radiocarbon ages obtained indicate that the Oldina slope deposits are largely a product of Pleistocene (periglacial) rather than Holocene processes. For example, the 14C ages obtained from the headwall of landslide 1 indicate periods of slope instability during MIS 3 (34.75 cal ka BP) and again during the LGM within MIS 2 (20.30 cal ka BP). Ages obtained at landslide 8 (27.45 cal ka BP and 15.58 cal ka BP), landslide 23 (16.77 cal ka BP) and landslide 6 (14.94 cal ka BP (MIS 2 deglacial period)) indicate multiple periods of instability within colluvial deposits, probably as a result of freeze-thaw processes. However, in several exposures, whether slope instability was caused by rapid movement (such as an earthflow) or by freeze-thaw processes could not be decided on the evidence available.

The angular nature of the stratified scree (grèze litées) in the backwall of landslide 23, and its stratification and age (16.77 cal ka BP) indicate a freeze-thaw origin, probably in a periglacial environment. Stratified screes are not well documented in Tasmania but appear to be quite common. Examples occur near Mathinna in the northeast (Caine 1983; Sharples 1994; McIntosh et al. 2009, 2012), in the Styx Valley in the south (Sharples 1997; McIntosh et al. 2012) and at Home Hill vineyard near Huonville where they have been dated in the range 21–26 cal ka BP (Table 1) (McIntosh et al. 2012), indicating that at least the Home Hill deposits formed during the LGM, the coldest and driest period of the
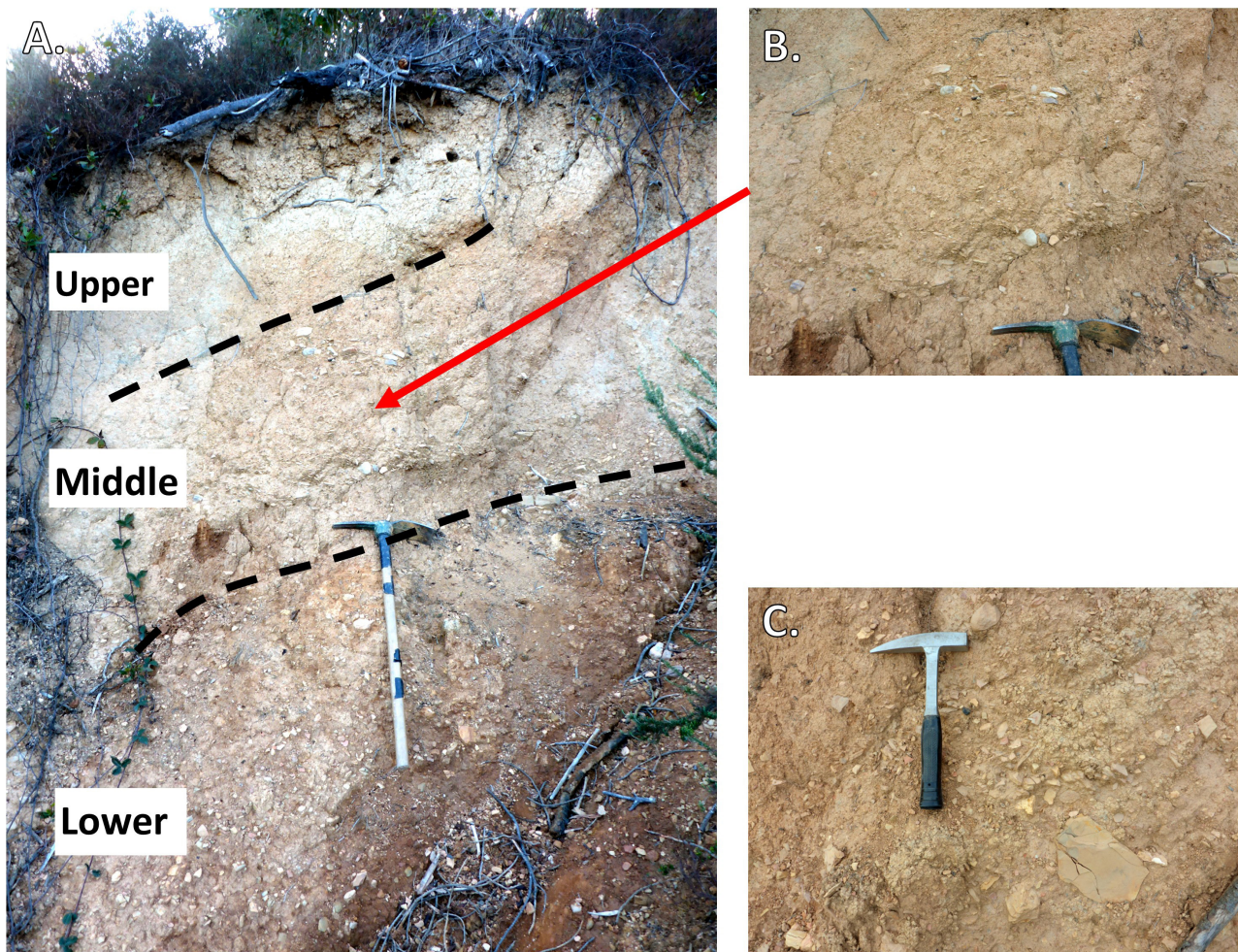
FIGURE 9: A. general view of sidewall of Landslide 8, showing three layers. Charcoal was scattered in the middle and lower layers. The pick is 90 cm long. B. The middle layer is interpreted to be of fluvial origin – note the imbrication of small stones. C. The chaotic lower layer, containing abundant angular stones, is interpreted to be either an old landslide deposit or a colluvial deposit formed by freeze-thaw processes.

Last Glacial period, in a sparsely vegetated landscape under a climate favouring rock fracturing and movement downslope by freeze-thaw processes. The 16.77 cal ka BP median age for the fine screes exposed in Landslide 23 is younger than the ages obtained at Home Hill (Table 1), indicating that at Oldina hillslope instability continued after the end of the LGM at about 17.5 ka BP (McIntosh et al. 2012), as also noted from the evidence of moraines and blockfields in Tasmania (Barrows et al. 2002, 2004; Mackintosh et al. 2006). It is likely that stratified screes formed from frost-prone Permian siltstone parent rock throughout MIS 2 in Tasmania, possibly intermittently after fires. The scarcity of charcoal in these stratified scree deposits confirms existence of tundra-like conditions at low altitudes in Tasmania to around 16.8 cal ka BP.

The radiocarbon ages obtained, coupled with observations of sediment characteristics, indicate widespread slope instability, particularly in the form of freeze-thaw processes, in the near-coastal Oldina region during the late Last Glacial period, when the climate was more continental due to the land bridge existing across

Bass Strait (Blom 1988), and when the overall climate in the Tasmanian region was not only colder but drier and supported drought-tolerant vegetation (McIntosh et al. 2009; Colhoun and Shimeld 2012; McIntosh et al. 2012, 2020).

Risk assessment and land management

Heavy rainfall is undoubtedly a major cause of mass movement (e.g., Tatard et al. 2010; Page et al. 2011; Garrido and Delgado 2013; Hong et al. 2017; Cogan et al. 2018; Qiu et al. 2019; Benz and Blum 2019). Most forested land was largely unaffected by the exceptional rainfall in June 2016, so it must be concluded that the unfortunate combination of recent forest harvest and heavy rain was the major contributor to the 2016 land instability in this geological terrain. Elsewhere heavy rain following natural fires has produced similar effects (e.g., Cannon et al. 2001; Shakesby & Doerr 2006; Nyman et al. 2011; Langhans et al. 2017; Rengers et al. 2020). Partial decomposition of roots (particularly fine roots) of the harvested pines (Watson et al. 1999; Ammann et al. 2009; Riley et al. 2013; Griffiths et al. 2020) was probably a factor contributing to instability at Oldina.
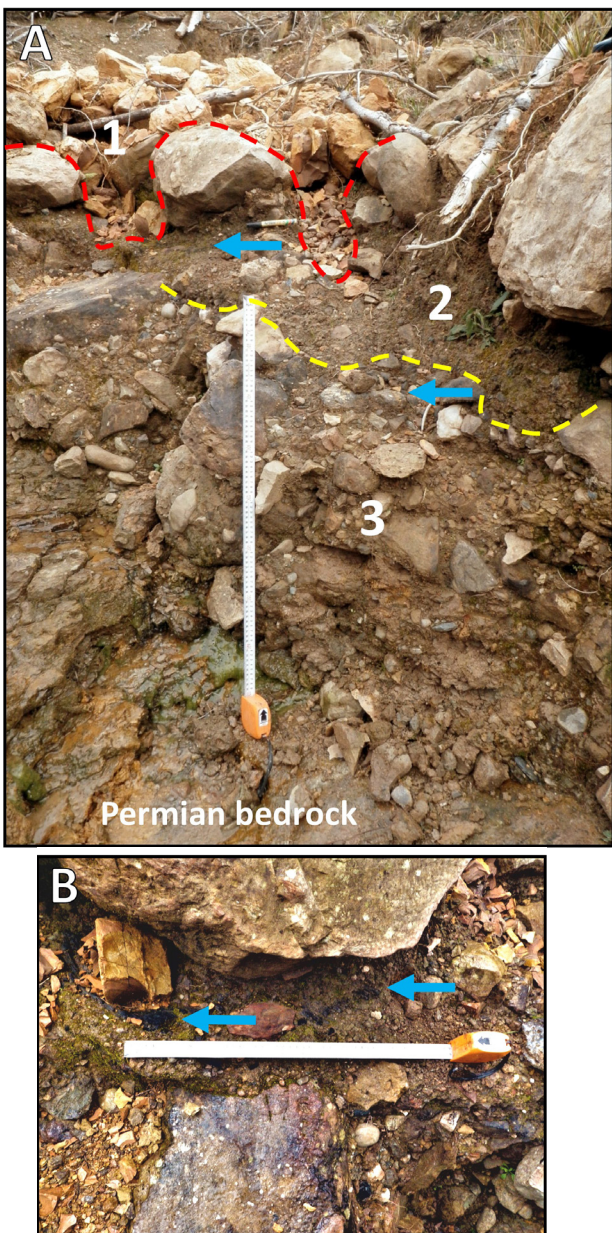
FIGURE 11: The backwall of Landslide 22. The outlined zone contains charcoal dated 1.94 cal ka BP (Table 1). It is likely to be the remains of a topsoil disturbed by mass movement, probably following a fire which baked the red-brown rocks in the lower horizon and those to the left of the tape. The top 1.1 m of the profile is soil that includes an A2 horizon. The tape is 2-m long.

FIGURE 10: A. The stratigraphy of the streambed at Landslide 18. The June 2016 debris forms Layer 1, a loose light brown stony layer. Blue arrows indicate charcoal layers. Layers 2 and 3 were radiocarbon dated, producing a median age of 0.18 cal ka BP and 1.05 cal ka BP for the top of each layer respectively (Table 1). Tape is 80-cm long; B. Detail of buried soil below rock in Layer 2. Tape is 50-cm long.

As has been shown in this study, landslides classified as shallow earthflows, rotational landslides, and translational landslides can generate and transport large volumes of material considerable distances from source: the 29 landslides documented at Oldina displaced a total mass of between 48400 and 72300 t of soil and rock, the bulk of which was stored on-site at the confluence of streams or behind log jams. However, as the mass of material generated by small riparian landslides, sheet,

gully, and rill erosion, or transported as suspended load downstream of the study site has not been accounted for, the calculation of the total mass of material (sediment and wood) generated is an underestimate. Furthermore, while the delivery of sediments and woody debris into Big Creek (the major stream draining the catchment) has in this instance been limited by on-site retention of sediment behind log jams, these log jams will in time disintegrate, releasing material into Big Creek and probably into the Inglis River estuary. To avoid recurrence of these erosion and stream sedimentation issues, mitigation strategies will be required to stabilise riparian slopes and limit the transport of sediment and woody-debris off-site via the stream network.

The Oldina landslides triggered a notification to the FPA, as required by the Tasmanian Forest Practices Code (FPA 2015) current at the time. The landslides directly impacted the plantation area, causing soil loss, loss of land availability for the next rotation, and the partial burial of access tracks and roads. In order to prevent long-term loss of land productivity (Blaschke et al. 2000) which can lead to property devaluation (Zumpano et al. 2018), and to stabilise riparian slopes, limit landslide expansion and prevent formation of new landslides, the company
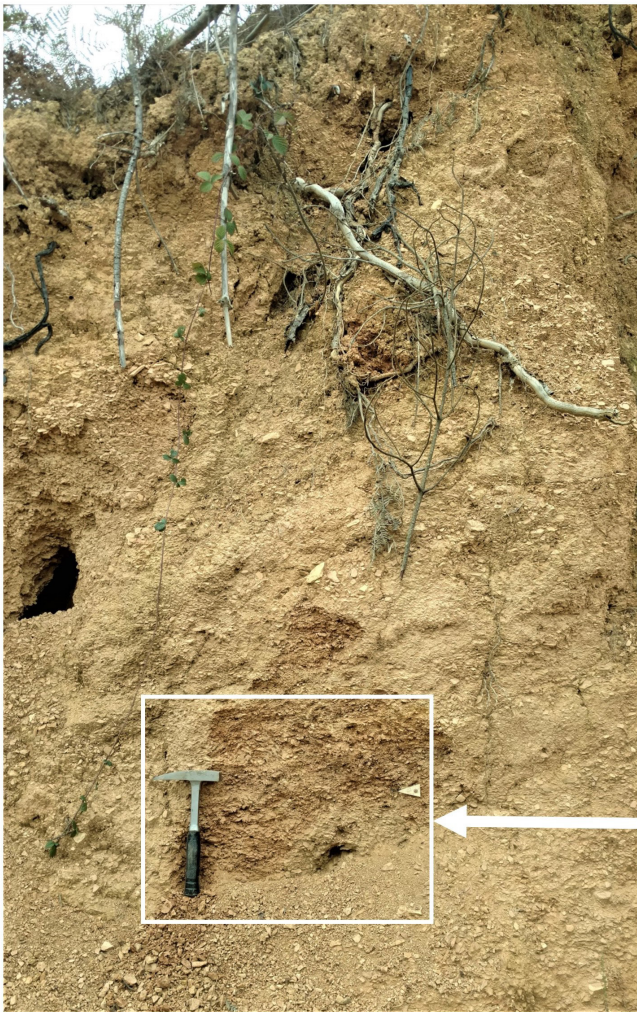
FIGURE 12: Landslide 23 formed by collapse of weakly stratified fine scree. On the sidewall of this landslide a thin band containing charcoal is indicated by the triangular marker. The median age of the charcoal (16.77 cal ka BP) indicates that the scree accumulated in a cold climate period (during MIS 2) as a periglacial deposit. The hammer is 27 cm long and the exposed section is about 1.5 m high.
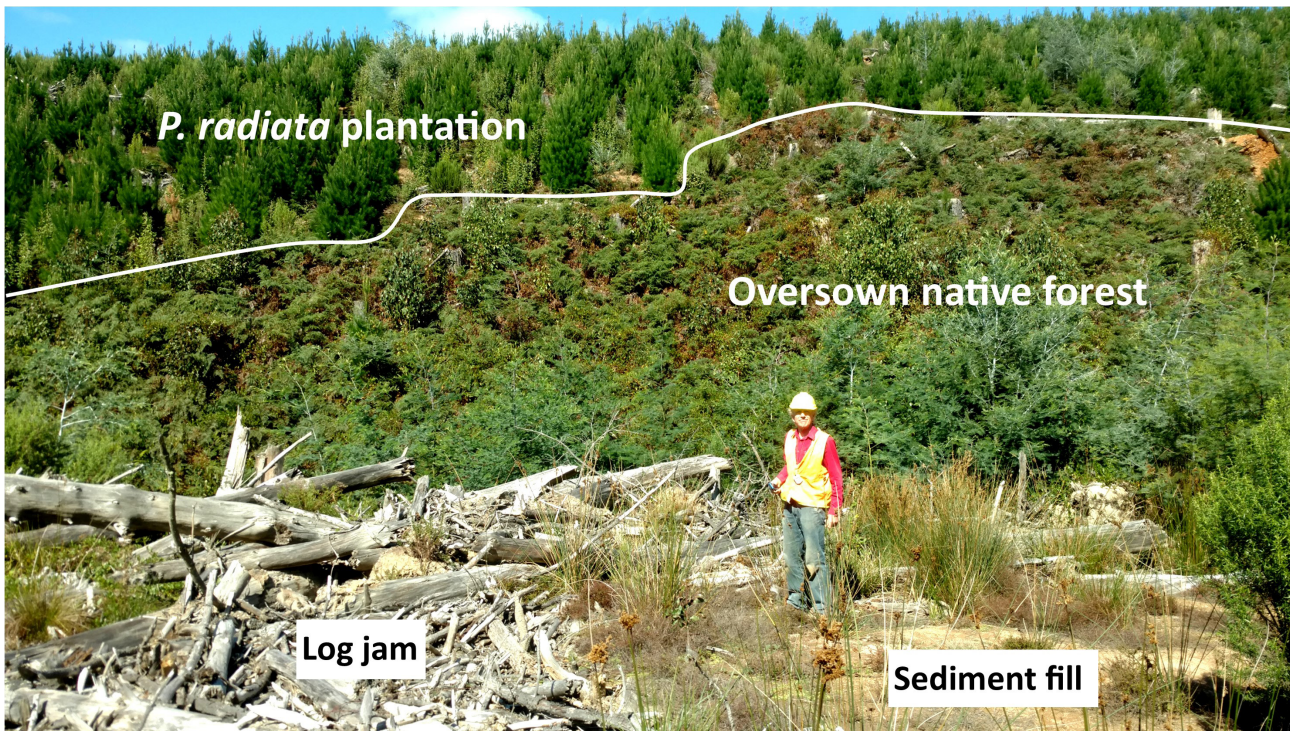

FIGURE 13: View of debris dam immediately downstream of Landslide 1. Riparian slopes have been re-established to native forest by oversowing and natural seed regeneration. Outside these areas a healthy *Pinus radiata* plantation has been established.

responsible for managing the Oldina plantations has, on the recommendation of the Forest Practices Authority, oversown all eroding slopes and all riparian zones with native tree species (*Eucalyptus obliqua* L'Hér., *Eucalyptus viminalis* Labill. and *Acacia melanoxylon* R.Br.) (Fig. 13).

It is noteworthy that White et al. (2010) predicted that with climate change the mean maximum 1-day rainfall intensities across the whole of Tasmania will increase by up to 35% in some coastal regions, especially in winter, and such changes are supported by the work of Grose et al. (2012), Gariano & Guzzetti (2016) and Nyman et al. (2019). These riparian protection measures, together with the protection provided by existing native riparian species such as *Leptospermum scoparium* J.R. et G.Forst. and *Dicksonia antarctica* Labill., should reduce the risk of future instability and provide long-term riparian and catchment protection (Schmidt et al. 2001; Roering et al. 2003; Ghestem et al. 2014; Stokes et al. 2014; Cohen and Schwarz 2017), and should be applied elsewhere in steep Permian tillite terrain.

Conclusions and Recommendations

Landslides initiated during exceptional rainfall in June 2016 represent the youngest of four periods of slope instability recorded at Oldina. Although there is evidence of limited mass movement during the late Holocene, when the climate was warm and wet and the Oldina area was forested, the Oldina landscape during this period is likely to have been mostly stable. The presence of layers of reddened soils and clasts in the headwalls of landslides suggests that any slope instability during the late Holocene was probably induced by natural fires and possibly the result of land clearance during early 19th century European colonisation rather than attributable to climatic factors.

The radiocarbon ages obtained suggest that the present-day landforms at Oldina are largely the product of widespread slope instability during the late Last Glacial period and result from the action of freeze-thaw processes on frost-prone Permian tillite parent rock when the overall climate in the Tasmanian region was not only colder but drier.

It is concluded that instability on these steeplands is not typical under the Holocene climate, but in this most recent instance was caused by unprecedented rainfall shortly after plantation harvest.

In view of the likelihood of high-intensity rainfall occurring more frequently in the future, and its inevitable occasional coincidence with forest harvest, greater riparian protection measures will be required on soils formed in Permian tillite and similar rock types, particularly where riparian zones are steep.

To improve long term steepland stability and plantation sustainability in Permian tillite terrain, all harvested landslide-prone riparian areas in the Oldina plantations have been oversown with native species and this policy is recommended on similar terrain elsewhere.

References

Ammann, M., Böll, A., Rickli, C., Speck T., & Holdenrieder, O. (2009). Significance of tree root decomposition for shallow landslides. *Forest, Snow and Landscape Research*, *82*(1), 79–94.

Bally, J. (2016). *Tasmanian record major flooding event – June 2016*, 65 pp. Melbourne, VIC: Bureau of Meteorology.

Barrows, T.T., Stone, J.O. & Fifield, K.L. (2004). Exposure ages for Pleistocene periglacial deposits in Australia. *Quaternary Science Reviews*, *23*(5–6), 697–708. https://doi.org/10.1016/j.quascirev.2003.10.011

Barrows, T.T., Stone, J.O., Fifield, K.L. & Cresswell, R.G. (2002). The timing of the Last Glacial Maximum in Australia. *Quaternary Science Reviews*, *21*(1–3), 159–173. https://doi.org/10.1016/S0277-3791(01)00109-3

Benz, S.A & Blum, P. (2019). Global detection of rainfall-triggered landslide clusters. *Natural Hazards and Earth System Sciences*, *19*, 1433–1444. https://doi.org/10.5194/nhess-19-1433-2019

Bermingham, K. (2016). Wynyard home will collapse after landslide moves ground below. *The Advocate*, June 12 2016.

Blaschke, P.M., Trustrum, N.A. & Hicks, D.L. (2000). Impacts of mass movement erosion on land productivity: a review. *Progress in Physical Geography*: *Earth and Environment*, *24*(1), 21–52. https://doi.org/10.1177/030913330002400102

Blom, W.M. (1988). Late Quaternary sediments and sea-levels in Bass Basin, southeastern Australia – a preliminary report. *Search, 19*(2), 94–96.

Bronk Ramsey, C. (2009). Bayesian analysis of radiocarbon dates. *Radiocarbon*, *51*(1), 337–360. https://doi.org/10.1017/S0033822200033865

Bureau of Meteorology (2016). Daily rainfall Yolla (Sea View) weather station, 5-6th June 2016. http://www.bom.gov.au/jsp/ncc/cdio/wData/wdata?p_nccObsCode=136&p_display_type=dailyDataFile&p_stn_num=091109&p_startYear=2016&p_c=-1660182508 accessed 5 April 2019

Bureau of Meteorology 2021a. Daily rainfall Wynyard Airport weather station 091367 http://www.bom.gov.au/jsp/ncc/cdio/weatherData/av?p_nccObsCode=136&p_display_type=dailyDataFile&p_startYear=&p_c=&p_stn_num=091367 accessed 23 November 2021

Bureau of Meteorology 2021b. Daily rainfall Yolla (Sea View) weather station 091109. http://www.bom.gov.au/jsp/ncc/cdio/weatherData/av?p_nccObsCode=136&p_display_type=dailyDataFile&p_startYear=&p_c=&p_stn_num=091109 accessed 23 November 2021

Burke, B., Slee, A., McIntosh, P.D., Hofmann, H. & Shulmeister, J. (2020). A reactivated cave system induces rapidly developing cover-collapse sinkholes in Tasmania, Australia. *Journal of Cave and Karst Studies*, *82*(1), 31–50. https://doi.org/10.4311/2019ES0109

Caine, N. (1983). *The mountains of northeastern Tasmania: a study of alpine geomorphology*. Salem, NH: Balkema.

Cannon, S.H., Kirkham, R.M. & Parise, M. (2001). Wildfire-related debris-flow initiation processes, Storm King Mountain, Colorado. *Geomorphology*, *39*(3–4), 171–188. https://doi.org/10.1016/S0169-555X(00)00108-2

Cogan, J., Gratchev, I. & Wang, G. (2018). Rainfall-induced shallow landslides caused by ex-Tropical Cyclone Debbie, 31st March 2017. *Landslides*, *15*, 1215–1221. https://doi.org/10.1007/s10346-018-0982-4

Cohen, D & Schwarz, M. (2017). Tree-root control on shallow landslides. *Earth Surface Dynamics*, *5*, 451–477. https://doi.org/10.5194/esurf-5-451-2017

Colhoun, E.A. & Shimeld, P.W. (2012). Late-Quaternary vegetation history of Tasmania from pollen records. In Haberle, S.G & David, B (Eds.), *Peopled Landscapes, Archaeological and Biogeographic Approaches to Landscapes*, *Terra Australis*, *34*, 297–328. https://doi.org/10.22459/TA34.01.2012.14

Dale-Glass Industries (2021). Timber Properties. https://dgi.com.au/timber-properties/ (Accessed 10 May 2021).

Dowdy, A.J., Mills, G.A. & Timbal, B. (2011). *Large-scale indicators of Australian East Coast Lows and associated extreme weather events.* [CAWCR Technical Report No. 037]. Aspendale,VIC: The Centre of Australian Weather and Climate Research.

Eberhard, R. (2016). Effect of an intense rainfall event in June 2016 on caves at Mole Creek, Tasmania. *Journal of the Australasian Cave and Karst Management Association*, *105*, 23–27.

Elliott, H. (2011). The early history of plantation forestry on State-owned land in Tasmania. *Tasforests, 19*, 71–85.

Elliott, H., Felton, K., Jarman, J. & Stone, M. (2008). *A History of Innovation: Eighty-five years of Research and Development at Forestry Tasmania*. Hobart, TAS: Forestry Tasmania.

Everard, J.L. (compiler) (2004). *Digital Geological Atlas 1:25000 Series, sheet 3845 Calder.* Rosny, TAS: Mineral Resources Tasmania.

Everard, J.L. & Calver, C.R. (compilers) (2006). *Digital Geological Atlas 1:25000 Series, sheet 3846 Wynyard*. Rosny, TAS: Mineral Resources Tasmania.

FAO (2014). World Reference Base for Soil Resources 2014. International soil classification system for naming soils and creating legends for soil maps. *World Soil Resources Report 106*. Rome: FAO.

Forest Practices Code (2020). Hobart, TAS: Forest Practices Authority.

García-Ruiz, J.M., Valero-Garcés, B., González-Sampériz, P., Lorente, A., Marti-Bono, C., Begueria, S. & Edwards, L. (2001). Stratified scree in the Central Spanish Pyrenees: palaeoenvironmental implications. *Permafrost and Periglacial Processes*, *12*(3), 233–242. https://doi.org/10.1002/ppp.388

Gariano, S.L. & Guzzetti, F. (2016). Landslides in a changing climate. *Earth-Science Reviews*, *162*, 227–252. https://doi.org/10.1016/j.earscirev.2016.08.011

Garrido, J. & Delgado, J. (2013). A recent, retrogressive, complex earthflow-earth slide at Cenes de la Vega, southern Spain. *Landslides*, *10*, 83–89. https://doi.org/10.1007/s10346-012-0358-0

Ghestem, M., Cao, K., Ma, W., Rowe, N., Leclerc, R., Gadenne, C. & Stokes, A. (2014). A framework for identifying plant species to be used as 'ecological engineers' for fixing soil on unstable slopes. *PLoS ONE*, *9*(8), e95876. https://doi.org/10.1371/journal.pone.0095876

Grant, J.C., Laffan, M.D., Hill, R.B. & Neilsen, W.A. (1995). Forest Soils of Tasmania. A handbook for identification and management. Hobart: Forestry Tasmania.

Griffiths, J.W., Lukens, C.E. & May, R. (2020). Increased forest cover and limits on clear-felling could substantially reduce landslide occurrence in Tasman, New Zealand. *New Zealand Journal of Forestry Science*, *50*(13). https://doi.org/10.33494/nzjfs502020x94x

Grose, M., Harris, R. & Lee, G. (2012). *A report to the Independent Verification Group for the Tasmanian*

Forest Agreement, IVG FC Report 6 Future Climate Projections. Hobart, TAS: Antarctic Climate and Ecosystems Cooperative Research Centre. https://www.environment.gov.au/system/files/resources/eefde0e6-0f83-486d-b0c3-8b1d25abc497/files/ivgconservation6climate.pdf

Henry, L.C., Isbell, J.L., Fielding, C.R., Domack, E.W., Frank, T.D. & Fraiser, M.L. (2012). Proglacial deposition and deformation in the Upper Carboniferous to Lower Permian Wynyard Formation, Tasmania: A process analysis. *Palaeogeography, Palaeoclimatology, Palaeoecology*, *315–316,* 142–157. https://doi.org/10.1016/j.palaeo.2011.11.020

Hill, R., Laffan, M. & Grant, J. (1995). Soils of Tasmanian State Forests. Forth Sheet, Soils Bulletin 3. Hobart, TAS: Forestry Tasmania.

Hirsch, F., Schneider, A., Bauriegel, A., Raab, A. & Raab, T. (2018). Formation, classification, and properties of soils at two relict charcoal hearth sites in Brandenburg, Germany. *Frontiers in Environmental Science*, *6*(94), 1–15. https://doi.org/10.3389/fenvs.2018.00094

Hogg, A., Heaton, T., Hua, Q., Palmer, J., Turney, C., Southon, J., Bayliss, A., Blackwell, P., Boswijk, G., Bronk Ramsey, C., Petchey, F., Reimer, P., Reimer, R. & Wacker, L. (2020). SHCal20 Southern Hemisphere calibration, 0-55,000 years cal BP. Radiocarbon, 62. https://doi.org/10.1017/RDC.2020.59

Hong, M., Kim, J & Jeong, S. (2017). Rainfall intensity-duration thresholds for landslide prediction in South Korea by considering the effects of antecedent rainfall. *Landslides*, *15*(5). https://doi.org/10.1007/s10346-017-0892-x

Kaine, C.L., Mazengarb, C. & Rigby, E.H. (2017). *The Caveside flood events of 2011 and 2016: A field investigation and modelling analysis.* Tasmanian Geological Survey Record UR2017/01. https://www.mrt.tas.gov.au/mrtdoc/dominfo/download/UR2017_01/UR2017_01.pdf

Kaine, C.L., Rigby, E.H. & Mazengarb, C. (2018). A combined morphometric, sedimentary, GIS and modelling analysis of flooding and debris flow hazard on a composite alluvial fan, Caveside, Tasmania. *Sedimentary Geology*, *364*, 286–301. https://doi.org/10.1016/j.sedgeo.2017.10.005

Langhans, C., Nyman, P., Noske, P.J., Van der Sant, R.E., Lane P.N.J. & Sheridan, G.J., (2017). Post-fire hillslope debris flows: Evidence of a distinct erosion process. *Geomorphology*, *295*, 55–75. https://doi.org/10.1016/j.geomorph.2017.06.008

Long, M. & Menkiti, C.O. (2007). Geotechnical properties of Dublin Boulder Clay. *Géotechnique*, *57*(7), 595–611. https://doi.org/10.1680/geot.2007.57.7.595

Lucieer, A., De Jong, S.M. & Turner D. (2013). Mapping landslide displacements using Structure from Motion (SfM) and image correlation of multi-temporal UAV photography. *Progress in Physical Geography*, *38*(1), 97–116. https://doi.org/10.1177/0309133313515293

Lynn, I.H. & Crippen, T.F. (1991). Rock type classification for the New Zealand Land Resource Inventory. *DSIR Land Resources Scientific Report 10*. Lower Hutt, NZ: DSIR Land Resources.

Mackintosh, A.N., Barrows, T.T., Colhoun, E.A. & Fifield, L.K. (2006). Exposure dating and glacial reconstruction at Mt. Field, Tasmania, Australia, identifies MIS 3 and MIS 2 glacial advances and climatic variability. *Journal of Quaternary Science 21(4)*, 363–376. https://doi.org/10.1002/jqs.989

Mazengarb, C & Stevenson, M.D. (2010). Tasmanian Landslide Map Series: User Guide and Technical Methodology. *Tasmanian Geological Survey Record 2010/01*.

Mazengarb, C., Stevenson, M.D. & Roberts, L. (2013). Landslide Planning Report. State Framework for Mitigation of Natural Hazards 12/11943, version 5. Hobart, TAS: Department of Premier and Cabinet.

McDonald, R.C., Isbell, R.F., Speight, J.G., Walker, J. & Hopkins, M.S. (1998). Australian soil and land survey field handbook. Canberra ACT: Department of Primary Industries and Energy and CSIRO.

McIntosh, P.D. (2016). *Earth Sciences report on Oldina and Oonah landslides and Kamona stream erosion following heavy rain, June 3–12, 2016.* Forest Practices Authority, Tasmania Report, 18 p.

McIntosh, P.D. & Barrows, T.T. (2011). Morphology and age of bouldery landslide deposits in forested dolerite terrain, Nicholas Range, Tasmania. *Zeitschrift für Geomorphologie*, *55*(3), 383–393. https://doi.org/10.1127/0372-8854/2011/0044

McIntosh, P.D., Price, D.M., Eberhard, R. & Slee, A.J. (2009). Late Quaternary erosion events in lowland and mid-altitude Tasmania in relation to climate change and first human arrival. *Quaternary Science Reviews*, *28*(9–10), 850–872. https://doi.org/10.1016/j.quascirev.2008.12.003

McIntosh, P.D., Eberhard, R., Slee, A., Moss, P., Price, D.M., Donaldson, P., Doyle, R. & Martins, J. (2012). Late Quaternary extraglacial cold-climate deposits in low and mid-altitude Tasmania and their climatic implications. *Geomorphology*, *179*, 21–39. https://doi.org/10.1016/j.geomorph.2012.08.009

McIntosh, P.D., Neudorf, C., Lian, O.B., Slee, A.J., Walker, B., Eberhard, R., Doyle, R & Dixon, G. (2020). Late Pleistocene and Early Holocene aeolian deposits of Tasmania and their climatic implications. *Quaternary Research*, *102*, 91–114. https://doi.org/10.1017/qua.2020.83

Miner, A.S., Flentje, P., Mazengarb, C., Selkirk-Bell, J.M. & Dalhaus, P. (2011). Some geomorphological techniques used in constraining the likelihood

of landsliding – selected Australian examples. *Australian Geomechanics Journal 46*(2), 7 p.

Mineral Resources Tasmania (2021). *Landslide Database.*

https://www.mrt.tas.gov.au/geoscience/engineering_geology/accordion/landslide_database accessed 24 June 2021

Nott, J.F., Thomas, M.F. & Price, D.M. (2001) Alluvial fans, landslides and Late Quaternary climatic change in the wet tropics of northeast Queensland. *Australian Journal of Earth Sciences 48*(6), 875–882. https://doi.org/10.1046/j.1440-0952.2001.00906.x

Nyman, P., Rutherfurd, I. D., Lane, P.N.J. & Sheridan, G.J. (2019). Debris flows in southeast Australia linked to drought, wildfire, and the El Niño-Southern Oscillation. *Geology, 47*(5), 491–494. https://doi.org/10.1130/G45939.1

Nyman, P., Sheridan, G.J., Smith, H.G. & Lane, P.N.J. (2011). Evidence of debris flow occurrence after wildfire in upland catchments of south-east Australia. *Geomorphology*, *125*(3), 383–401. https://doi.org/10.1016/j.geomorph.2010.10.016

Page, M.J., Langridge, R.M. & Jones, K.E. (2011). *The December 2011 Debris Flows in the Pohara-Ligar Area, Golden Bay.* Lower Hutt, New Zealand: GNS Science https://www.gns.cri.nz/Home/Our-Science/Natural-Hazards-and-Risks/Landslides/Project-Examples/Golden-Bay-Debris-Flows

Panek, T. (2015). Recent progress in landslide dating: A global review. *Progress in Physical Geography*, *39*(2), 168–198. https://doi.org/10.1177/0309133314550671

Peruccacci, S., Brunetti, M. T., Gariano, S.L., Melillo, M., Rossi, M & Guzzetti, F. (2017). Rainfall thresholds for possible landslide occurrence in Italy. *Geomorphology*, *290*, 39–57. https://doi.org/10.1016/j.geomorph.2017.03.031

Pook, M., Risbey, J & McIntosh, P. (2010). East coast lows, atmospheric blocking and rainfall: a Tasmanian perspective. 17th National Conference of the Australian Meteorological and Oceanographic Society, IOP Conf. Series. *Earth and Environmental Science*, *11*(012011), 6 p. https://doi.org/10.1088/1755-1315/11/1/012011

Qiu, H., Cui, Y., Hu, S., Yang, D., Pei, Y. & Yang, W. (2019). Temporal and spatial distributions of landslides in the Qinba Mountains, Shaanxi Province, China. *Geomatics*, *Natural Hazards and Risk*, *10*(1), 599–621. https://doi.org/10.1080/19475705.2018.1536080

Rengers, F.K., McGuire, L.A., Oakley, N.S., Kean, J.W., Staley, D.M. & Tang, H. (2020). Landslides after wildfire: initiation, magnitude, and mobility. *Landslides*, *17*, 2631–2641. https://doi.org/10.1007/s10346-020-01506-3

Riley, K.L., Bendick, R., Hyde, K.D. & Gabet, E.J. (2013).

Frequency-magnitude distribution of debris flows compiled from global data, and comparison with post-fire debris flows in the western U.S. *Geomorphology*, *191*, 118–128. https://doi.org/10.1016/j.geomorph.2013.03.008

Roering, J.J., Schmidt, K.M., Stock, J.D., Dietrich, W.E. & Montgomery, D.R. (2003). Shallow landsliding, root reinforcement, and the spatial distribution of trees in the Oregon Coast Range. *Canadian Geotech Journal*, *40*, 237–253. https://doi.org/10.1139/t02-113

Schmidt, K.M., Roering, J.J., Stock, J.D., Dietrich, W.E., Montgomery, D.R. & Schaub, T. (2001). The variability of root cohesion as an influence on shallow landslide susceptibility in the Oregon Coast Range. *Canadian Geotechnical Journal*, *38*(5), 995–1024. https://doi.org/10.1139/t01-031

Shakesby, R.A. & Doerr, S.H. (2006). Wildfire as a hydrological and geomorphological agent. *Earth-Science Reviews*, *74*(3–4), 269–307. https://doi.org/10.1016/j.earscirev.2005.10.006

Sharples, C. (1994). *A reconnaissance of landforms and geological sites of geoconservation significance in the north-eastern Tasmanian forest districts.* Report to Forestry Tasmania vol.2. Hobart, TAS: Forestry Tasmania. 134 p.

Sharples, C. (1997). *A reconnaissance of landforms and geological sites of geoconservation significance in the western Derwent forest district.* Report to Forestry Tasmania. Hobart, TAS: Forestry Tasmania. 114 pp.

Slee, A & Shulmeister, J. (2015). The distribution and climatic implications of periglacial landforms in eastern Australia. *Journal of Quaternary Science*, *30*(8), 848–858. https://doi.org/10.1002/jqs.2823

Slee, A., McIntosh, P. & Barrows, T. (2017). Using [36]Cl exposure dating to date mass movement and assess land stability on the Nicholas Range, Tasmania. *Landslides*, *14*(6), 2147–2154. https://doi.org/10.1007/s10346-017-0868-x

Slee, A., McIntosh, P., Webb, J., Sharples, C. & Williams, K. (2019). Managing geomorphic values within Tasmanian plantations on karst terrain. *Australian Forestry*, *82*(3), 127–138. https://doi.org/10.1080/00049158.2019.1656704

Stevenson, P.D. (2011). Grasping the nettle - The Tasmanian Geological Survey's work on landslides, 1971–1988. *Papers and Proceedings of the Royal Society of Tasmania*, *145*, 39–49. https://doi.org/10.26749/rstpp.145.39

Stevenson, M.D. & Mazengarb, C. (2010). Tasmanian Landslide Map Series: User Guide and Technical Methodology. Report UR2010_01. Hobart, TAS: Mineral Resources Tasmania.

Stokes, A., Douglas, G.B., Fourcaud, T., Giadrossich, F., Gillies, C., Hubble, T., Kim, J.H., Loades, K.W., Mau, Z., McIvor, I.R., Mickovski, S.B., Mitchell, S., Osman, N., Phillips, C., Poesen, J., Polster, D., Preti, F., Raymond, P., Rey, F., Schwarz, M. & Walker, L.R. (2014). Ecological mitigation of hillslope instability: ten key issues facing researchers and practitioners. *Plant and Soil*, *377*(1–2), 1–23. https://doi.org/10.1007/s11104-014-2044-6

Sutherland, F.L. & Wellman, P. (1986). Potassium-argon ages of Tertiary volcanic rocks, Tasmania. *Papers and Proceedings of the Royal Society of Tasmania*, *120*, 77–86. https://doi.org/10.26749/rstpp.120.77

Tatard, L., Grasso, J.R., Helmstetter, A. & Garambois, S. (2010). Characterization and comparison of landslide triggering in different tectonic and climatic settings. *Journal of Geophysical Research*, *115*(F04040). https://doi.org/10.1029/2009JF001624

Tulau, M.J., Nyman, P., Young, M., Morand, D., McInnes-Clarke, S.K. & Noske, P. (2019). Mass movements of Warrumbungle National Park, New South Wales, Australia. *Proceedings of the Linnean Society of New South Wales, 141,* S11–S130.

Turner, D., Lucieer, A. & de Jong, S.M. (2015). Time Series Analysis of Landslide Dynamics Using an Unmanned Aerial Vehicle (UAV). *Remote Sensing*, *7*, 1736–1757. https://doi.org/10.3390/rs70201736

Ulery, A.L. & Graham, R.C. (1993). Forest Fire Effects on Soil Color and Texture, Division S-5—Soil Genesis, Morphology & Classification. *Soil Science Society of America Journal*, *57*(1), 135–140. https://doi.org/10.2136/sssaj1993.03615995005700010026x

United States Geological Service (USGS) (2004). Landslide Types and Processes. *Fact Sheet 2004-3072*.

https://pubs.usgs.gov/fs/2004/3072 (accessed 19/3/2021)

Watson, A., Phillips, C. & Marden, M. (1999). Root strength, growth, and rates of decay: root reinforcement changes of two tree species and their contribution to slope stability. *Plant and Soil*, *217*, 39–47. https://doi.org/10.1023/A:1004682509514

White, C.J., Grose, M.R., Corney, S.P., Bennett, J.C., Holz, G.K., Sanabria, L.A., McInnes, K.L., Cechet, R.P., Gaynor, S.M. & Bindoff, N.L. (2010). *Climate futures for Tasmania Extreme Events Technical Report.* Hobart, TAS: Antarctic Climate and Ecosystems Cooperative Research Centre.

Wirsu, P. (2017). Mersey Forest Road destroyed by landslips. *The Examiner, June 5 2017*.

Zumpano, V., Pisano L., Malek, Z., Micu, M., Aucelli, P.P.C., Rosskopf, C.M., Balteanu, D. & Parise, M. (2018). Economic losses for rural land value due to landslides. *Frontiers in Earth Science*, *6*(97), 1–13. https://doi.org/10.3389/feart.2018.00097